Simulation of full-scale reverse osmosis filtration system for the removal of N-nitrosodimethylamine from wastewater

M. A. Al-Obaidi [1, 2], C. Kara-Zaïtri [1] and I. M. Mujtaba [1, *]

[1] Chemical Engineering Division, School of Engineering, University of Bradford. Bradford, West Yorkshire BD7 1DP, UK

[2] Middle Technical University, Iraq – Baghdad

***Corresponding author, Tel.: +44 0 1274 233645**

E-mail address: I.M.Mujtaba@bradford.ac.uk

Abstract

Reverse osmosis (RO) is becoming one of the most promising technologies used in wastewater treatment because it offers high rate of contaminant rejection and lower energy consumption in comparison with other thermal treatment processes. Earlier research by the same authors in respect of a distributed one-dimensional mathematical model for a single spiral-wound RO membrane module based on the solution-diffusion model has been used in this paper to simulate the rejection of NDMA (N-nitrosodimethylamine) from wastewater in a series of seven RO elements full-scale treatment plant. Firstly, the applicability of this model has been evaluated using a simulation study and the results have been compared against experimental data gathered from the literature for a given plant. Secondly, further simulation and analysis studies are carried out to assess the performance of the plant for NDMA rejection and recovery rate under different operating conditions of feed pressure, flow rate, and concentration. For the studied RO configuration, it is concluded that a maximum of 55.1% NDMA rejection can be achieved, which confirms the remaining issue of lower NDMA rejection.

Keywords: Reverse Osmosis; Spiral-wound membrane; Modelling; Full-scale RO plant; Wastewater Treatment; N-nitrosamine Removal.

1. Introduction

Reverse Osmosis (RO) is a water purification process, used in water desalination and wastewater treatment. RO uses a semipermeable membrane to remove undesirable particles. The rapid

growth of RO membrane technology in wastewater treatment is attributed to a number of factors including high packing density, minimum thermal damage, do not involve phase change, and lower energy consumption with its simplicity of operation and maintenance. [1,2] Furthermore, spiral-wound RO modules are known to be relatively easy to clean with a lower fouling possibility. [3,4]

Nitrosamine and specifically N-nitrosodimethylamine (NDMA) is an organic compound, which has been detected in chlorinated water and addressed as a probable human carcinogen. The removal of NDMA from water is becoming a real challenge due to low-molecular weight of NDMA with high hydrophilic properties. Generally, ozone and chlorine oxidants are effectively used to abate NDMA from wastewater because of its efficiency to destroy amines. However, this high-cost process may lead to form NDMA in special cases and circumstances. For example, the existence of ammonia in wastewater can hinder the efficiency of chlorination oxidation treatment due to forming chloramine, which can easily react with other nitrogen compounds to form NDMA. [5]

On the line of this research, the efficiency of the Reverse Osmosis (RO) process to remove NDMA from wastewater was particularly in the range 40 – 70%. [6]

To the best of authors' knowledge, Fujioka *et al.*[7] and Al-Obaidi *et al.* [8] are the only researchers who have attempted the development of Spiegler and Kedem based models to estimate the performance of the spiral-wound RO process when removing N-nitrosamine compounds from wastewater. It is also believed that the influence of the operating parameters on the development of a distributed mathematical model for the rejection of NDMA nitrosamine based on the solution-diffusion model have yet to be achieved, especially for the case of a full-scale plant of a series of seven RO elements.

In this research, the earlier work of the same authors in respect of a one-dimensional mathematical model is used to predict the variation of operating parameters along the x-axis of a spiral-wound RO element and to estimate the total NDMA nitrosamine rejection for a series configuration of seven RO elements full-scale plant working under specified operating parameters. The model is based on the solution-diffusion principle. The consistency of this model has been corroborated by a validation study using experimental data gathered from the literature. Also, the performance of NDMA rejection and recovery rate of the plant have been analysed foe variable operating conditions of feed pressure, flow rate, and concentration.

2. Modelling of spiral-wound reverse osmosis

The performance of a spiral wound RO process is mainly dependent on the operating conditions of the process. The optimisation of this process can reduce the cost of treatment, which is readily required the development of a distributed package model. This type of models can obtain a realistic insight of the operating parameters' variation, which preserves the optimisation process. [9] A one-dimensional model, which includes the physical properties equations, has been developed for an individual spiral-wound RO system by Al-Obaidi *et al.* [10] for the removal of organic compounds from wastewater. The model has been calibrated to estimate the total NDMA nitrosamine rejection of a series of seven elements RO pilot-plant. The model equations are conveniently presented in Table 1 for a spiral wound membrane module, which schematic diagram is shown in Fig. 1.

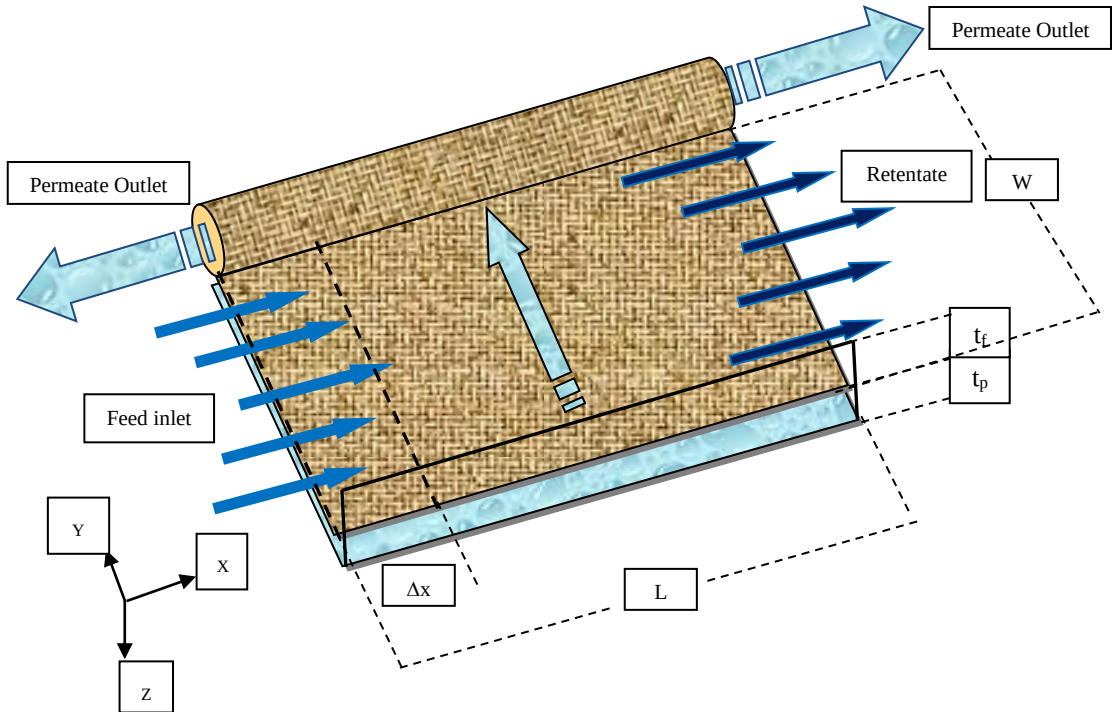

Fig. 1. Schematic diagram of a spiral wound membrane module

Table 1. Equations describing the spiral-wound RO model of Al-Obaidi *et al.* [10]

Model Equations	Specifications	Eq. no.
$F_{b(x)} = \left\{F_{b(0)} - \left(W\ \theta\ x\ \Delta P_{b(0)}\right) + \left(W\ \theta\ b\ \left(\frac{x^2}{2}\right)\ F_{b(0)}\right) + \left(W\ \theta\ b\ \left(\frac{W\ \theta}{b}\right)^{0.5}\left(\frac{x^2}{2}\right)\ \left(\Delta P_{b(x)} - \Delta P_{b(0)}\right)\right)\right\}$	Calculate feed flow rate at any point along the x-axis	1
$\theta = \frac{A_w\ B_s}{B_s + R\ T_b\ A_w\ C_{p(av)}}$	Parameter in Eq. (1)	2
$U_{b(x)} = \frac{F_{b(x)}}{t_f\ W}$	Calculate feed velocity at any point along the x-axis	3
$P_{b(x)} = \left\{P_{b(0)} - \left(b\ x\ F_{b(0)}\right) + \left(b\ W\theta\ \left(\frac{x^2}{2}\right)\left(\Delta P_{b(x)}\right)\right) - \left[b^2\ W\theta\ \left(\frac{x^3}{6}\right)F_{b(0)}\right] - \left[b^2\ W\ \theta\ \left(\frac{W\ \theta}{b}\right)^{0.5}\left(\frac{x^3}{6}\right)\ \left(\Delta P_{b(x)} - \Delta P_{b(0)}\right)\right]\right\}$	Calculate feed pressure at any point along the x-axis	4
$\Delta P_{b(x)} = \Delta P_{b(0)} - \left(b\ x\ F_{b(0)}\right) - \left[\left(\frac{W\ \theta}{b}\right)^{0.5} b\ x\ \left(\Delta P_{b(x)} - \Delta P_{b(0)}\right)\right]$	Calculate pressure difference between the feed and permeate channels at any point along the x-axis	5
$J_{w(x)} = \theta\ \left\{\left[\Delta P_{b(0)} - \left(b\ x\ F_{b(0)}\right)\right] - \left[\left(\frac{W\ \theta}{b}\right)^{0.5} b\ x\ \left(\Delta P_{b(x)} - \Delta P_{b(0)}\right)\right]\right\}$	Calculate water flux at any point along the x-axis	6
$J_{s(x)} = B_s\ (C_{w(x)} - C_{p(av)})$	Calculate the solute flux at any point along the x-axis	7
$\frac{(C_{w(x)} - C_{p(av)})}{(C_{s(x)} - C_{p(av)})} = exp\left(\frac{J_{w(x)}}{k_{(x)}}\right)$	Calculate wall solute concentration at any point along the x-axis	8
$k_{(x)} = 0.753\ \left(\frac{K}{2-K}\right)^{0.5}\left(\frac{D_{b(x)}}{t_f}\right)\left(\frac{\mu_{b(x)}\ \rho_{b(x)}}{D_b}\right)^{0.1666}\left(\frac{2\ t_f^2\ U_{b(x)}}{D_b\ \Delta L}\right)^{0.5}$	Calculate mass transfer coefficient at any point along the x-axis	9
$\mu_{b(x)} = 1.234E-6\ exp\left\{0.0212x10^{-3}\ C_{s(x)}\ (18.0153) + \frac{1965}{T_b + 273.15}\right\}$	Calculate viscosity at any point along the x-axis	10
$\rho_{b(x)} = 498.4\ m_{f(x)} + \sqrt{\left[248400\ m_{f(x)}^2 + 752.4\ m_{f(x)}\ C_{s(x)}\ (18.0153)\right]}$	Calculate density at any point along the x-axis	11
$m_{f(x)} = 1.0069 - 2.757E-4\ T_b$	Calculate $m_{f(x)}$ at any point along the x-axis	12
$\frac{C_{s(x)}}{t_f\ W}\frac{dF_{b(x)}}{dx} + \frac{F_{b(x)}}{t_f\ W}\frac{dC_{s(x)}}{dx} = \frac{d}{dx}\left[D_b\ \frac{dC_{s(x)}}{dx}\right] - \frac{(J_{w(x)}\ C_{p(x)})}{t_f} + \frac{(J_{w(x)}\ C_{s(x)})}{t_f}$	Calculate feed solute concentration at any point along the x-axis	13
$C_{p(av)} = \frac{C_{p(0)} + C_{p(L)}}{2}$	Calculate average permeate solute concentration	14
$C_{p(0)} = \frac{B_s\ C_{s(0)}\ e^{\frac{J_{w(0)}}{k(0)}}}{J_{w(0)} + B_s\ e^{\frac{J_{w(0)}}{k(0)}}}$ and $C_{p(L)} = \frac{B_s\ C_{s(L)}\ e^{\frac{J_{w(L)}}{k(L)}}}{J_{w(L)} + B_s\ e^{\frac{J_{w(L)}}{k(L)}}}$	Calculate permeate solute concentrations at x=0 and x=L	15, 16
$F_{p(x)} = F_{p(0)} + \left(W\ x\ \theta\ \Delta P_{b(0)}\right) - \left[W\ \theta\ b\ \left(\frac{x^2}{2}\right)F_{b(0)}\right] - \left[W\ \theta\ b\ \left(\frac{x^2}{2}\right)\left(\frac{W\ \theta}{b}\right)^{0.5}\ \left(\Delta P_{b(x)} - \Delta P_{b(0)}\right)\right]$	Calculate permeated flow rate at any point along the x-axis	17
$Rec_{(Total)} = \frac{F_{p(L)}}{F_{b(0)}} x\ 100$ $Rej = \frac{C_{s(0)} - C_{p(av)}}{C_{s(0)}} x100$	Calculate total water recovery and solute rejection	18, 19

Eqs. (1) to (19) describe the process of transport phenomena of permeate and solute through a single spiral-wound RO membrane module and the associated physical properties equations.

The feed flow rate $F_{b(x)}$ reduces along the membrane length, which can be calculated using Eq. (1). While, Eq. (3) provides the velocity $U_{b(x)}$ at any point along the x-axis. The pressure at the feed channel $P_{b(x)}$ and the pressure difference $\Delta P_{b(x)}$ between the feed and permeate channels are decreased due to the friction at the membrane surface and calculated using Eqs. (4) and (5) respectively. The water $J_{w(x)}$ and solute fluxes $J_{s(x)}$ through the membrane are calculated using Eqs. (6) and (7) respectively. Specifically, the membrane surface is exposed to a concentration, $C_{w(x)}$, which is greater than the solution bulk concentration due to the concentration polarization phenomenon. The concentration polarization impact is included using the film theory model of Eq. (8). The mass transfer coefficient $k_{(x)}$ was estimated using the empirical correlation of Mane *et al.* [11] given Eq. (9). The requirements of physical properties, viscosity $\mu_{b(x)}$ and density $\rho_{b(x)}$ parameters have been calculated using Eqs. (10), (11) and (12) as reported by Koroneos [12]. While, the diffusivity parameter of NDMA D_b is given in Table 2 at 20 °C. The calculation of solute concentration $C_{s(x)}$ along the feed channel is conducted using the proposed correlation of Lee *et al.* [13] of Eq. (13). Also, the average permeate solute concentration $C_{p(av)}$ of both the inlet $C_{p(0)}$ and outlet permeate concentrations $C_{p(L)}$ were calculated using Eqs. (14), (15) and (16) respectively. The permeate flow rate $F_{p(x)}$ at any point along the x-axis of permeate channel is calculated using Eq. (17). Also, the total recovery $Rec_{(Total)}$ of the system and NDMA nitrosamine rejection Rej are estimated using Eqs. (18) and (19) respectively.

The model code of a spiral-wound reverse osmosis membrane module has been implemented on the gPROMS software suite [14] in a steady state mode, where the feed side is divided into several sections of equal intervals (Δx) as shown in Fig. 1.

3. Materials and methods

A full-scale RO filtration system consisting of seven 4″ glass-fiber pressure vessels of a commercial thin film composite reverse osmosis membrane packed into a spiral wound module (Make: Hydranautics, Oceanside, CA., USA) was used by Fujioka *et al.* [7] in their experimental work to remove NDMA (N-nitrosodimethylamine-D6) from wastewater. Filtration experiments were carried out using 250E-6 ppm as the NDMA feed concentration. The analytical method

used by Fujioka *et al.* [7] included solid phase extraction (SPE), followed by gas chromatography and analysis by tandem mass spectrometry with electron impact ionisation. The reader is referred to Fujioka *et al.* [7] for further investigation of the analytical method.

The retentate-reprocessing design is used where the retentate of the first vessel was reprocessed at the second vessel followed by the third one. Moreover, the permeate of all the vessels is blended to form the total permeate and recycled back with the retentate stream into the feed tank to sustain a constant feed concentration along the treatment experiments. The feed was pumped at a constant volumetric flow rate of 2.43E-3 m^3/s using a pump type (CRN 3-25, Grundfos, Bjerringbro, Denmark), and pressure of 6.5 atm. The feed temperature was specified at 20 ± 0.1 °C using an electrical boiler. Fig. 2 shows a schematic diagram of the full-scale plant of seven RO elements used by Fujioka *et al.* [7] While, the characteristics of the spiral-wound membrane element are given in Table 2.

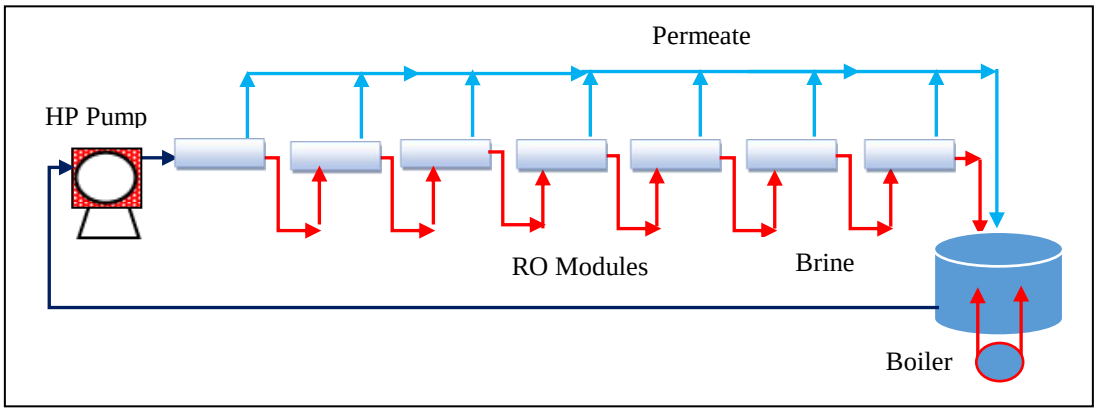

Fig. 2. Schematic diagram of full-scale seven elements RO plant used by Fujioka *et al.* [7]

Table 2. Specifications of the spiral-wound membrane element used by Fujioka *et al.* [7]

Make	Hydranautics, Oceanside, CA., USA
Membrane type and configuration	ESPA2-4040, Spiral-wound, Composite Polyamide
Feed and permeate spacer thickness t_f (m)	6.6E-4
Membrane sheet area (m^2)	7.9
Membrane sheet length L and width W (m)	0.9 and 8.7778
Characteristic length of spacer ΔL (m)	0.006
The efficiency of mixing K (dimensionless) *	0.5
Diffusion coefficient of NDMA D_b at 20 °C (m^2/s)	9.7E-10

*: Mane *et al.* [11]

4. Determination of transport parameters

The determination of the unknown parameters of the proposed model in addition to the operating parameters are key when solving the model equations. This section therefore discuses the prediction of these unknown parameters.

The experimental data of Fujioka *et al.* [7] will be used to estimate the best values of unknown parameters, which are then used with the known model parameters to study the impact of the operating variables on system performance. In the present experiment of initial conditions of 6.51 atm, 2.43E-3 m³/s, 250 ppm and 20 ºC, the model unknown parameters A_w, B_s and b were found using the gEST parameter estimation technique in the gPROMS for each RO element in a series of seven elements considering the experimental data and the variation of inlet operating conditions for each element. The water permeability constant A_w varies between 1.0 to 1.22E-6 m/s atm, while the solute transport parameter B_s varies between 5.15 to 5.67E-6 m/s. As a result, Eqs. (1) and (2) were developed to estimate the water and NDMA transport parameters. This is compared to the assumption of constant values of A_w and B_s as 1.4E-6 m/s atm and 5.35E-6 m/s respectively, which were made by Fujioka *et al.* [7] considering the rejection of NDMA. In addition, Eq. (3) is developed to calculate the friction parameter b relating to the average Reynolds number along the membrane length. The impact of temperature on both water and solute transport parameters are not included in the equations developed because there was no experimental data for the temperature influence.

$$A_w = 0.3333\left\{\left(2E-7\,P_{b(0)}\right)+\left(0.0013\,F_{b(0)}\right)-\left(785.44\,C_{s(0)}\right)+2.1E-6\right\} \quad (20)$$

$$B_s = 0.3333\left\{\left(3E-7\,P_{b(0)}\right)+\left(0.0023\,F_{b(0)}\right)-\left(1364.6\,C_{s(0)}\right)+1.406E-5\right\} \quad (21)$$

$$b = 1.8052\,Re_{(av)} - 793.46 \quad (22)$$

$$Re_{(x)} = \frac{2\,\rho_{b(x)} t_f\, U_{b(x)}}{\mu_{b(x)}} \quad (23)$$

5. Model validation

The model described in Section 2 has been tested using a comparison between the model predictions and those obtained from actual experimentation for the specific pilot-plant of seven

RO membranes in a series configuration. Fig. 3 shows the comparative analysis of the outlet feed pressure, outlet permeate flux, NDMA rejection, NDMA outlet feed concentration, and NDMA average permeate concentration between the experimental results and the model predictions. Overall, the predicted values of the model for the retentate pressure, and water flux along the x-axis of seven elements in a series configuration are in a good agreement with experimental data. However, it looks like the model is over-estimating the retentate concentrations and the permeate concentration of the elements especially at the last membrane by a maximum error of 16% and 18.8% respectively. Having said this, ignoring the impact of the fouling factor in the proposed model may reduce the efficiency of the prediction of these specified parameters, where the water permeability constant has ignored the fouling impact. This, in turn results in reducing the accuracy of the model prediction for retentate and permeate concentrations, where the water and solute transport parameters have a significant impact. Most importantly, the model prediction of the rejection parameter is within a maximum error of 6.3%. The model is explored further by simulation as reported in the next section.

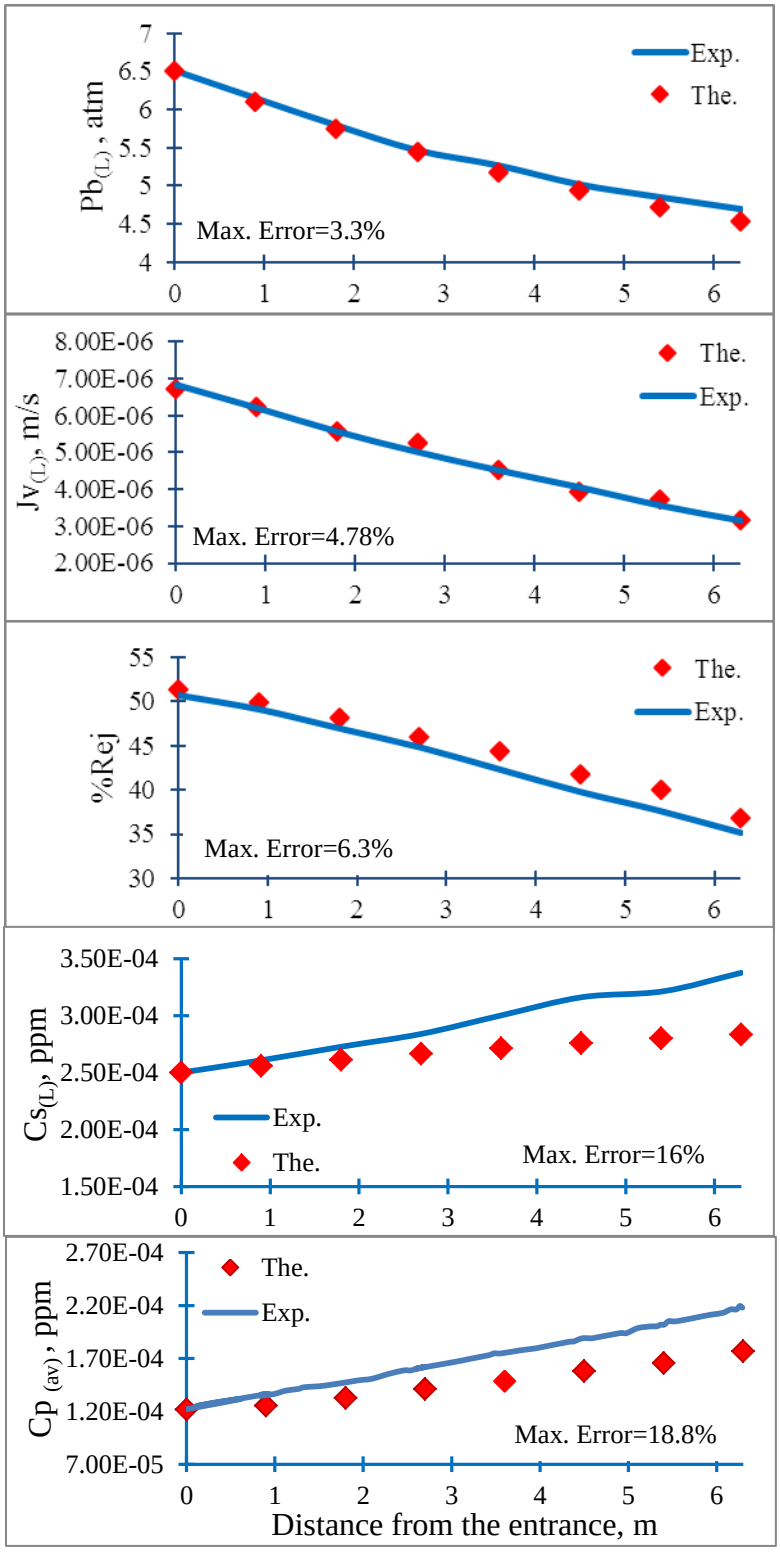
Pb(L), atm
Exp.
The.
Max. Error=3.3%
Jv(L), m/s
Max. Error=4.78%
%Rej
Max. Error=6.3%
Cs(L), ppm
Max. Error=16%
Cp (av), ppm
Max. Error=18.8%
Distance from the entrance, m

Fig. 3. Experimental and model prediction of (a) outlet feed pressure, (b) outlet permeate flux, (c) NDMA rejection, (d) NDMA outlet feed concentration and (e) NDMA average permeate concentration (feed conditions: 6.51 atm, 250E-6 ppm, 2.43E-3 m³/s and 20 ºC)

6. Analysis the impact of operating parameters on the plant performance

Here, the model is used to simulate the process, and evaluate its sensitivity to different parameters of the process, and take an overview of the total NDMA rejection and recovery rate for the RO plant of a series of seven elements while of varying the process parameters.

The response of the total NDMA rejection and recovery rate for the variation in both inlet feed pressure of 4 to 18 atm and feed flow rate of 7.85E-4 to 2.5E-3 m³/s are shown in Figs. 4 and 5 for the case of constant operating conditions of inlet feed concentration and temperature of 250E-6 ppm and 20 ºC respectively. The total water recovery is already can be used to recognise the total water flux of the seven modules of the configuration tested.

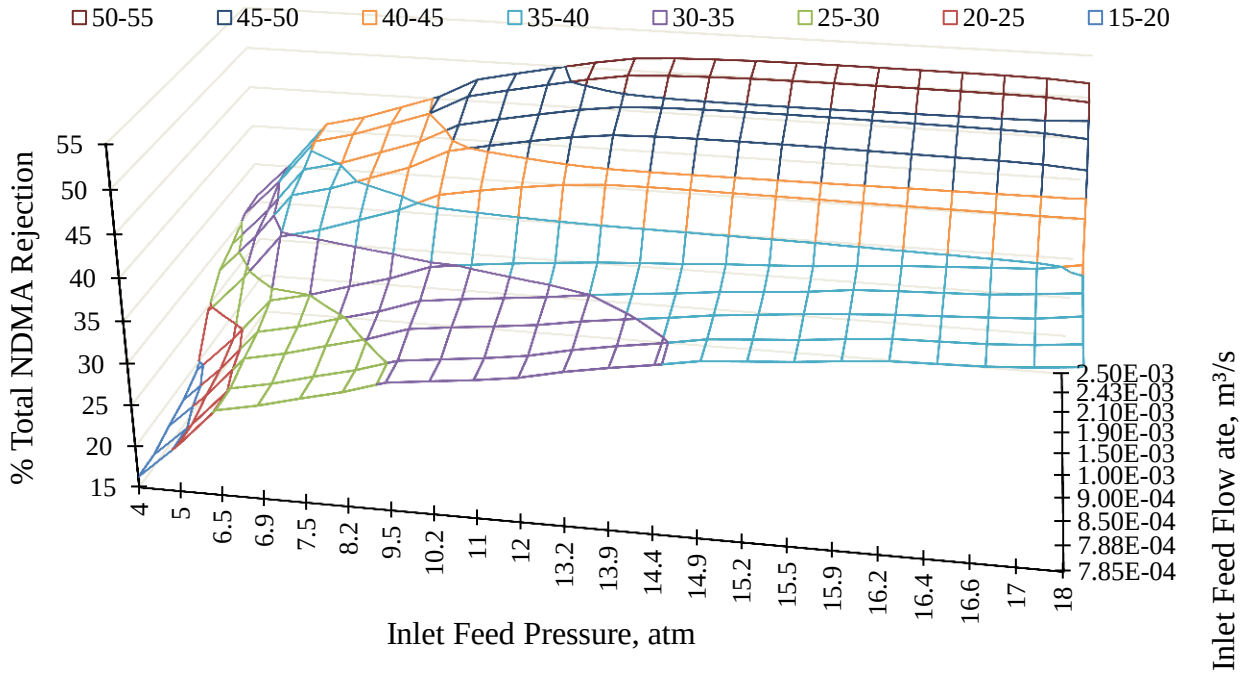

Fig. 4. Impact of variation in feed pressure and flow rate on total NDMA rejection at fixed inlet feed concentration and temperature (250E-6 ppm and 20 ºC)

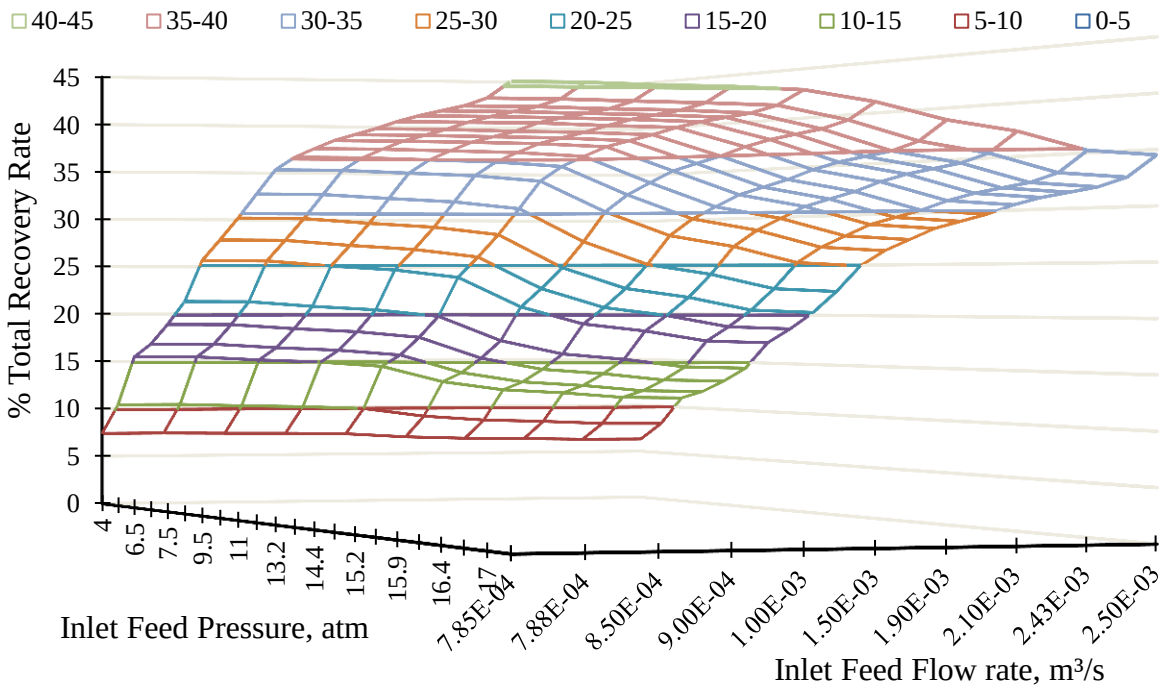

Fig. 5. Impact of variation in feed pressure and flow rate on total recovery rate at fixed inlet feed concentration and temperature (250E-6 ppm and 20 ºC)

It can readily be seen from Fig. 4 that the maximum NDMA rejection is approximately 52%, which is achieved at the operating conditions of 2.5E-3 m³/s and 15.9 atm for the set used of inlet feed pressure and flow rate respectively. Interestingly, Fig. 4 shows that the total NDMA rejection increases as a result of an increase in the operating pressure especially at low feed flow rates conditions. This is due to an increase in the water flux caused by increasing the operating feed pressure, (already shown in Fig. 5), which reduces solute concentration in the permeate channel and enhances the rejection parameter. However, Fig. 4 indicates that the progress of operating pressure at the range of 1.5E-3 to 2.5E-3 m³/s of feed flow rate can cause a little reduction in the NDMA rejection and this is caused by an increase in the concentration and the osmotic pressure of the feed side, which reduces the flux of water through the membrane. This concern can be clearly seen in Fig. 5 where a slight reduction in the total recovery rate occurs at the range of 1.5E-3 to 2.5E-3 m³/s of feed flow rate. It can be argued therefore that Fig. 4 affirms the existence of an optimised operating pressure commensurate with the highest NDMA rejection for the set of operating conditions tested. However, at the lower range of feed flow rate

(7.85E-4 to 1.5E-3 m^3/s), the progress of feed pressure gradually enhances the NDMA rejection, with an approximately constant water recovery (Fig. 5).

It can also be argued that increasing the total NDMA rejection caused by an increase in the feed flow rate is readily attributed to a reduction of the osmotic pressure. This in turn increases the mass transfer coefficient, which reduces the concentration polarization effect and feed concentration at the membrane wall. The proposed model shown in Table 1 has already taken into consideration the concentration polarisation impact by assuming the validity of the film theory model required for estimating the membrane wall concentration (Table 1, Eq. 8). Sutzkover *et al.* [15] have confirmed the suitability of using such simplified thin film model to investigate the concentration polarisation. However, this time, it is permissible to use a higher feed flow rate to guarantee a higher total NDMA rejection rather than using low feed flow rate as with other methods. The reason behind low rejections at operating conditions of low feed flow rates and operating pressures is that in such conditions, there is a lower driving force of water flux but with a higher impact of concentration polarization.

Statistically, at the optimum operating conditions of 2.5E-3 m^3/s and 15.9 atm commensurate with the maximum NDMA rejection, Fig. 4 shows that the variation of feed flow rate from 7.85E-4 to 2.5E-3 m^3/s can positively impact the rejection parameter by around 41%. Similarly, the feed pressure variation from 4 to 18 atm can reinforce the rejection rate by around 67%.

Fig. 5 confirms that the process can generate a maximum recovery rate of around 40% at the operating condition of the highest pressure tested and the lowest tested feed flow rate of 18 atm and 7.85E-4 m^3/s respectively. It is not difficult to see that an increase in the feed pressure causes a significant increase in the recovery rate because of underlying lift of the quantity of water flux. However, there is a clear reduction in the recovery rate as a result to an increase in the operating feed flow rate, especially after 1E-3 m^3/s. The explanation of this is an increase in the pressure drop per each element as a response to an increase in the operating flow rate. This in turn leads to a reduction of the driving force of water flux in addition to a reduction of the residence time of feed inside the module.

The response of the total NDMA rejection for the variation in both inlet feed pressure of 4 to 18 atm and inlet feed concentration of 74.05E-6 to 370.25E-6 ppm at constant feed flow rate and temperature of 8.5E-4 m^3/s and 20 °C (case 1) respectively are given in Fig. 6. While, Fig. 7

shows the same above operating conditions at higher and constant feed flow rate of 2.43E-3 m³/s (case 2).

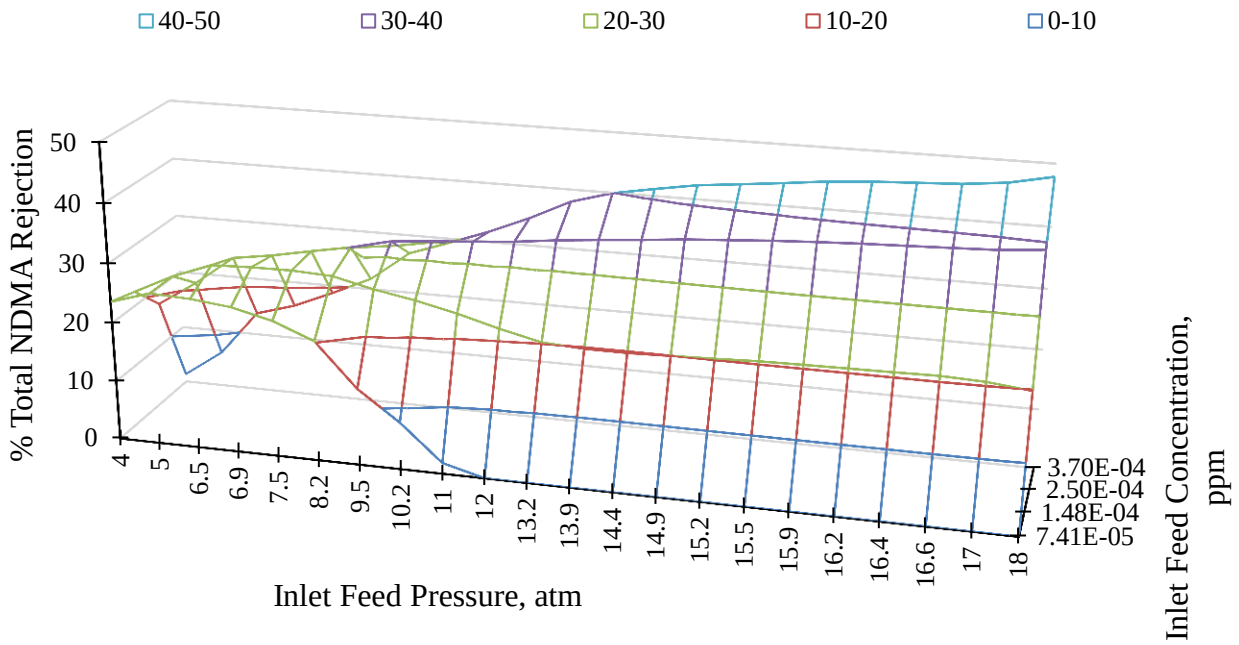

Fig. 6. Impact of variation in feed pressure and concentration (case 1) on total NDMA rejection at fixed inlet feed flow rate and temperature (8.5E-4 m³/s and 20 ºC)

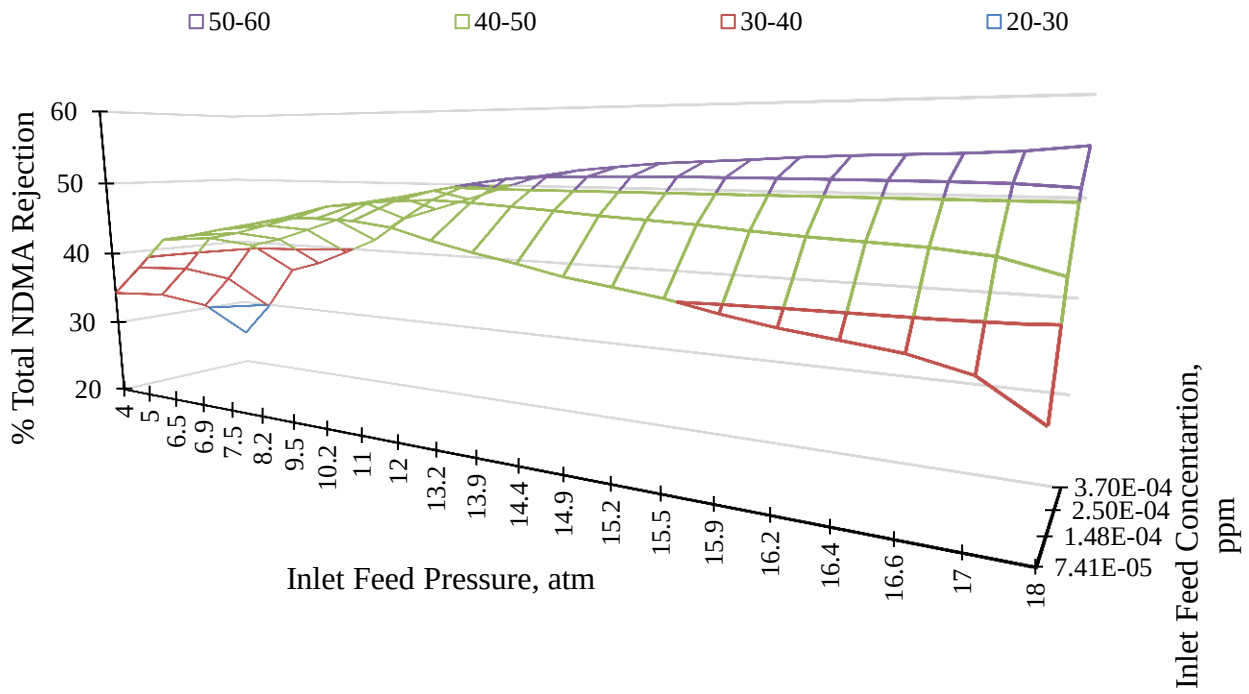

Fig. 7. Impact of variation in feed pressure and concentration (case 2) on total NDMA rejection at fixed inlet feed flow rate and temperature (2.43E-4 m^3/s and 20 ºC)

A close look at the results of Figs. 6 and 7 shows that the maximum total NDMA rejection is around 55.1%, which is achieved at the highest tested operating conditions of feed pressure and concentration of 18 atm and 370E-6 ppm respectively. The maximum value of NDMA rejection can reflect the poor performance of the RO process for the removal of NDMA, which has been readily confirmed in several studies including. [16,17,6,7]

Interestingly, Figs 6 and 7 show that at low and high operating feed flow rate of 8.5E-4 and 2.43E-3 m^3/s and low range of operating pressures of 4 to 8.5 atm, the total NDMA rejection decreases as a result to an increase in the operating concentration. Also, it can be said that there is a specific value of feed concentration that can achieve optimum NDMA rejection especially after 4 atm. Haluch *et al.* [18] confirmed that the feed concentration has a considerable impact on rejection parameter, where there is an optimal value, which provides the maximum rejection for a small-capacity desalination unit working at low feed flow rate and pressure. From this statement, it can be derived that at a range of low operating pressures (4 to 8.5 atm), the feed concentration behaves harmoniously with the total NDMA rejection rate regardless the feed flow rate used. This can be attributed to the increase in the osmotic pressure as a response to the increase in the feed concentration, which immediately reduces the water flux and rejection

parameter. Also, it can be noted that the process performance of rejection parameter can be improved when operating at low feed concentrations and low range of operating pressures especially at higher feed flow rate (Fig. 7). This is due to mitigating the concentration polarization impact at lower feed concentrations and high feed flow rate, which increases the mass transfer coefficient and the total permeated water. However, Figs 6 and 7 confirm that this statement is overlapped after increasing the feed pressure beyond 8.5 atm. It is easy to see that the total NDMA rejection is significantly increased due to an increase in the operating concentration. This phenomenon is related to the quantity of water flux that can penetrate the membrane as a result of an increase in the operating pressure. Broadly speaking, the NDMA permeate concentration reduces due to an increase in the operating pressure as a result of an increase the driving force of water flux. Moreover, increasing the operating concentration can reinforce the total NDMA rejection in the range of high operating feed pressure up to 8.5 atm. The following observation can be made: increasing the membrane solute isolation intensity as a response to an increase in the feed concentration [19] or due to recognizing that an increase in the feed concentration results in an increase in the bulk concentration, which is incomparable to the low concentration at the permeate channel. Therefore, the rejection parameter increases by increasing the feed concentration as can be verified in Eq. (19) in Table 1. This conclusion is similar to the findings of Gómez *et al.* [20]

The total NDMA rejection at the operating conditions of low feed concentration of 74.1E-6 ppm, high operating pressures, and low operating feed flow rate of 8.5E-4 m^3/s is reduced to zero as can be verified in Fig. 6 and gradually reduced at high operating feed flow rate of 2.43E-3 m^3/s as can be verified in Fig. 7. This can be explained as follows: it is expected that operating at high pressure will result in a higher permeate flux. However, it seems that the impact of low inlet feed flow rate is more noticeable at these conditions by encouraging the concentration polarization and increasing the flux of solute through the membrane. This in turn will retard the total NDMA rejection. However, a simple comparison between Figs. 6 and 7 can support the conclusion that it is perfectly permissible this time to use higher feed flow rate to guarantee the RO performance of removing the NDMA. This is based on the fact that operating at high feed flow rate can enhance the mass transfer coefficient and periodically alleviate the rejection parameter.

The findings of the previous section motivate further investigation of the relation existing between the feed concentration and flow rate at fixed operating pressures more particularly for

the performance of a series configuration of seven elements of the RO process for the NDMA removal from wastewater. The next section provides a detailed analysis about this aspect.

Figs. 8, 9 and 10 clearly illustrate the impact of operating feed flow rate and concentration variations of 7.85E-04 to 2.5E-3 m^3/s and 74.1E-6 to 370E-6 ppm respectively for three cases of constant operating pressure of 6.51, 10 and 18 atm at constant temperature of 20 °C. Fig. 11, on the other hand, shows the impact of the same above variation on the total water recovery at fixed pressure and temperature of 18 atm and 20 °C respectively.

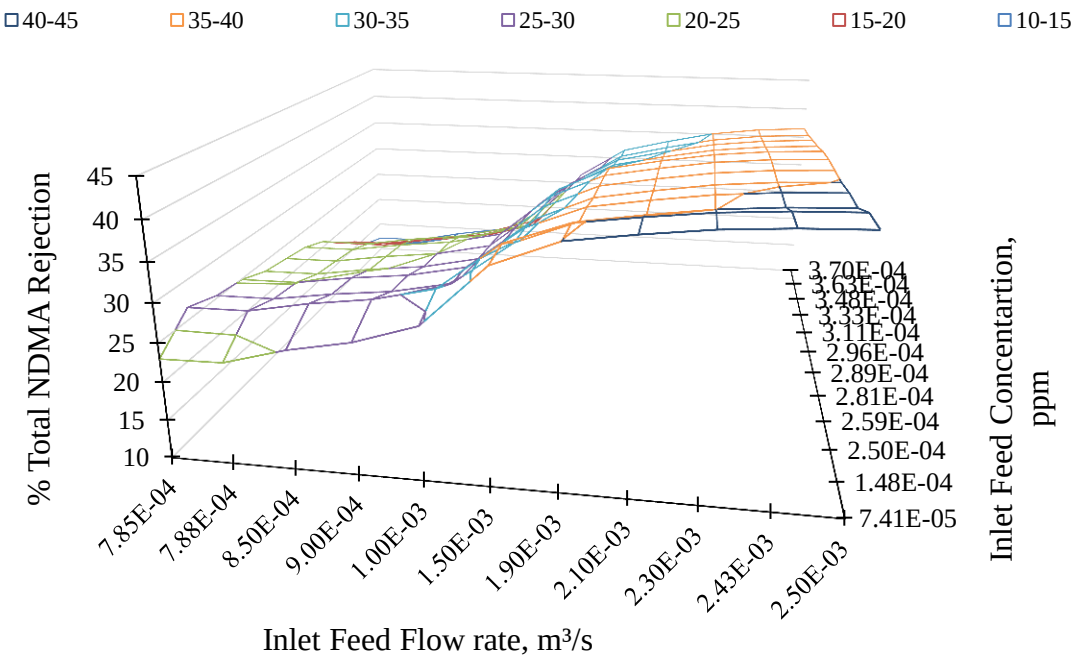

Fig. 8. Impact of variation in feed concentration and flow rate on total NDMA rejection at fixed inlet feed pressure and temperature (6.51 atm and 20 *°C*)

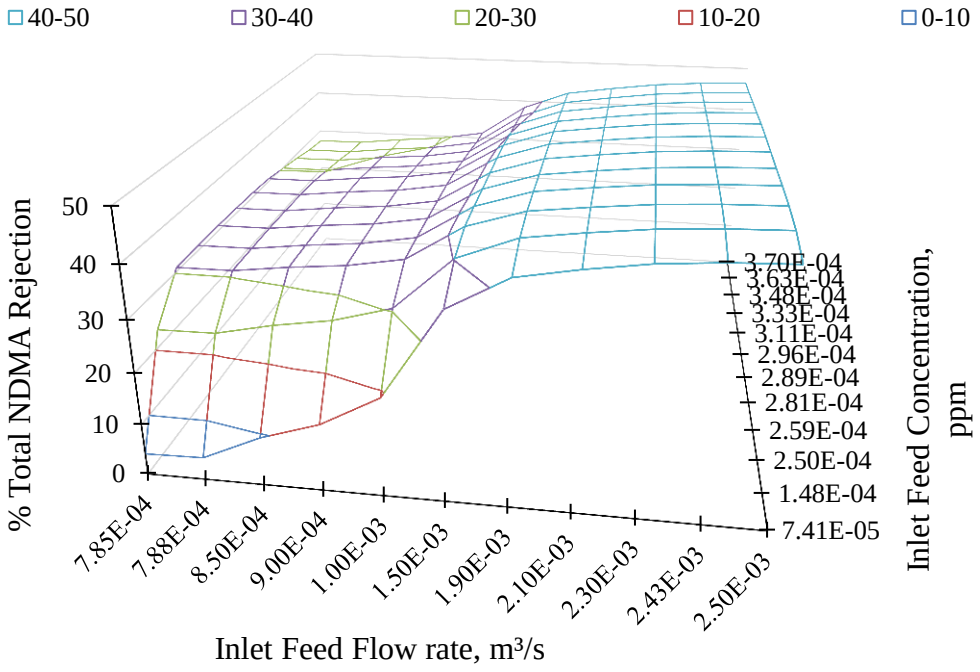

Fig. 9. Impact of variation in feed concentration and flow rate on total NDMA rejection at fixed inlet feed pressure and temperature (10 atm and 20 *ºC*)

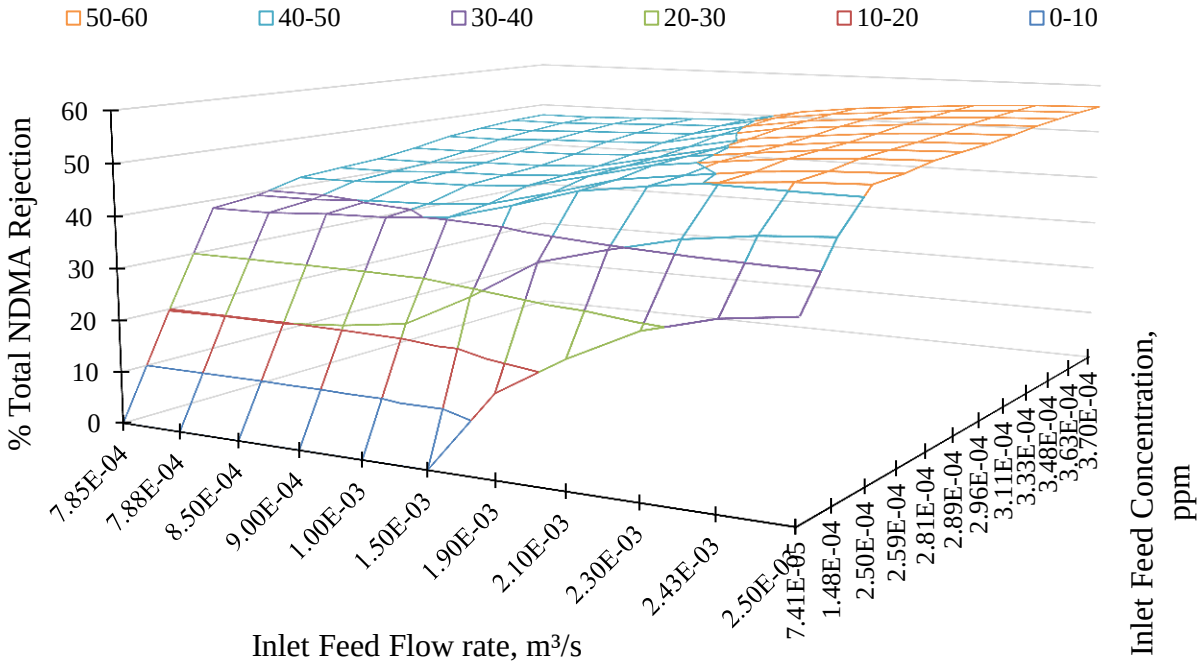

Fig. 10. Impact of variation in feed concentration and flow rate on total NDMA rejection at fixed inlet feed pressure and temperature (18 atm and 20 *ºC*)

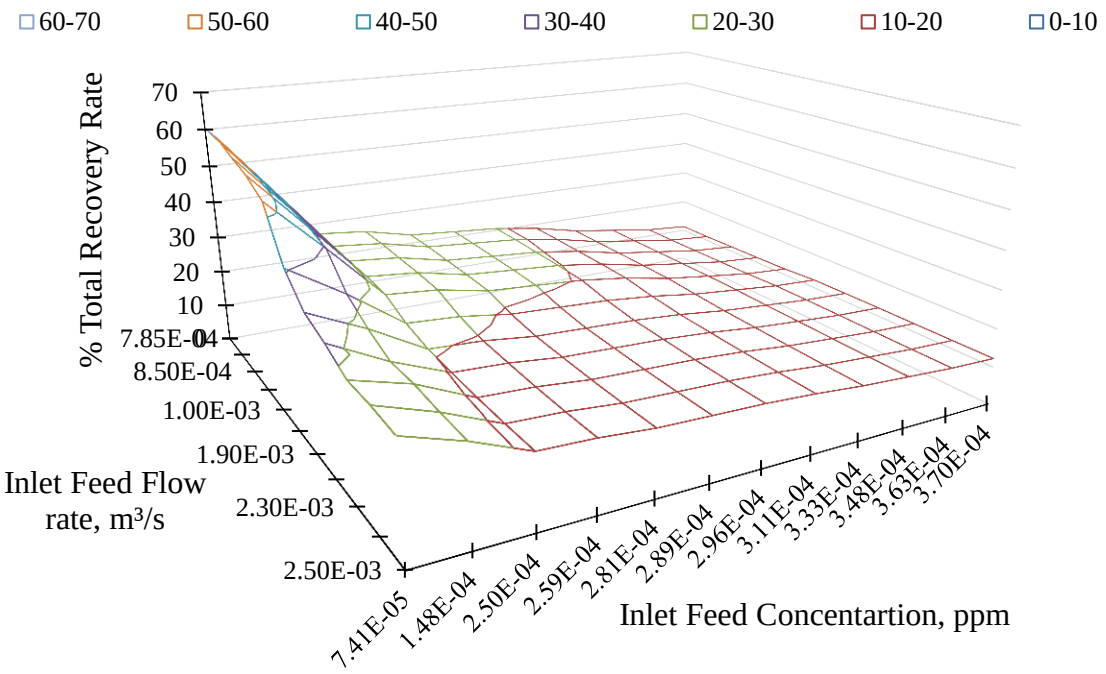

Fig. 11. Impact of variation in feed concentration and flow rate on total recovery rate at fixed feed pressure and temperature (10 atm and 20 *ºC*)

Firstly, Figs 8 and 9 easily show that the maximum registered total NDMA rejection increases as a consequence to increasing the operating pressure from 6.5 to 10 atm by about 42.87% and 48.49% respectively. The optimum NDMA rejections are totally achieved at operating conditions of feed flow rate of 2.5E-3 m³/s and concentration of 74.1E-6 ppm and 250E-6 ppm in the case of using operating pressure of 6.51 and 10 atm respectively. However, Fig. 10 shows that the maximum rejection of 55.4% comes at 370E-6 ppm for the case of using operating pressure of 18 atm and 2.5E-3 m³/s of feed flow rate. Therefore, it can be concluded that the maximum NDMA rejection is always achieved at the highest feed flow rate regardless the operating pressure.

Statistically, the simulation results of Fig. 8 show that the total NDMA rejection is reduced by about 14.8% from 42.87% to 36.5% for a variation of feed concentration from 74.1E-6 ppm to 250E-6 ppm respectively, where 74.1E-6 ppm represents the optimum concentration of a maximum rejection of 42.87%. While, the variation of feed flow rate from 7.85E-4 m³/s to 2.5E-4 m³/s causes a significant increase in the rejection parameter by about 85.9% from 23% to 42.87%. Also, Fig. 8 shows that the maximum NDMA rejection in the case of using low operating pressure of 6.51 atm is achieved at the lowest concentration used. This is because of

lower impact of concentration polarisation that can be occur at lower feed concentrations, which in turn lifts the water flux as clearly indicated by Fig. 11. Moreover, Fig. 11 confirms that lower feed concentration always results with the highest recovery rate at all the feed flow rates tested for the same aforementioned reason. Fig. 11 shows that the feed flow rate has a noticeable impact on total water recovery at the lower range of feed concentrations. This is compared to the insignificant impact of feed flow rate on the recovery rate at the upper tested range of inlet feed concentrations.

Similarly, the maximum NDMA rejection occurs at feed concentration of 250E-6 ppm and 2.5E-3 m^3/s when using the higher feed pressure of 10 atm (Fig. 9). Again, this case can reflect the same previous complementary actions of feed flow rate and operating concentration to control NDMA rejection at the middle range of operating pressures. However, the feed flow rate variation from 7.85E-4 m^3/s to 2.5E-4 m^3/s has increased the rejection parameter by 57.7% from 30.74% to 48.49%, where 2.5E-4 m^3/s represents the optimum feed flow rate of maximum rejection of 48.49%. It also be noting that the feed concentration variation of 74.1E-6 ppm to 250E-6 ppm has a negative impact of less than 1% on the NDMA rejection parameter, where 250E-6 ppm is the optimum concentration of maximum rejection. Moreover, another contradiction of the two cases of 6.51 atm and 10 atm shown in Figs. 8 and 9 is that the maximum rejection of 10 atm occurred in a specific optimum concentration. Interestingly, at these conditions of maximum NDMA rejection, Fig. 11 shows the lower recovery rate that can be achieved at these conditions.

Finally, running the process at the highest feed pressure of 18 atm can deviate the monitoring of maximum NDMA rejection, where the process shows that the feed concentration has a significant positive impact on the rejection parameter (compared to the cases of 6.51 and 10 atm) considering the feed flow rate influence. Statistically, the simulation results of Fig. 10 show that the variation of feed concentration from 74.1E-6 ppm to 370E-6 ppm has a positive impact of about 63% on total NDMA rejection, where 370E-6 ppm is the optimum concentration of the highest rejection of 55.4%. This is compared to a positive impact of 16.6% on total NDMA rejection caused by a variation from 7.85E-4 m^3/s to 2.5E-4 m^3/s of feed flow rate, where 2.5E-4 m^3/s represents the optimum flow rate of maximum rejection. Also, the simulation results of running the process at the operating conditions of 18 atm and 370E-6 ppm at the set of 7.85E-4

to 2.5E-3 m^3/s of feed flow rate have confirmed the insignificant impact of feed flow rate on total recovery rate, where the recovery rate yields approximately a constant value of 24%.

Figs 9 and 10 clearly show that running the process at a range of low feed flow rates of 7.85E-4 to 1.5E-3 m^3/s and low feed concentration has dropped noticeably the NDMA rejection regardless of the operating pressures of 10 and 18 atm respectively. This can be explained by recognising that the low feed flow rate can actually enhance the accumulation of solute over the membrane wall, which in turn increases the solute flux accompanied to water flux and deteriorates the permeate concentration. However, the rejection parameter is dramatically increased after 1.5E-3 m^3/s for all the tested operating concentrations.

Generally, the total water recovery decreases as a result to an increase in operating concentration and flow rate as can be shown in Fig. 11. The variations of pressure 74.1E-6 ppm to 370E-6 ppm and flow rate 7.85E-4 m^3/s to 2.5E-4 m^3/s at the optimum operating conditions of maximum recovery rate of 74.1E-6 ppm and 7.85E-4 m^3/s causes a decrease in water recovery by about 81% and 53% respectively. The increase of osmotic pressure as a result to the increase in the operating concentration and the reduction of time residence of the feed inside the module may explain this phenomenon.

Finally, Fig. 12 shows the progress of total NDMA rejection through the seven RO elements of full-scale plant under operating conditions of inlet feed flow rate of 7.85E-04 to 2.5E-3 m^3/s with fixed feed concentration, pressure, and temperature of 250E-6 ppm, 10 atm and 20 ^oC respectively. In general, NDMA rejection deteriorates along the series RO membranes for all the set of operating feed flow rate due to changes in hydrodynamic states and solution properties in the subsequent feed and permeate channels. Again, Fig 12 confirms the importance of using high feed flow rate to encourage the NDMA rejection.

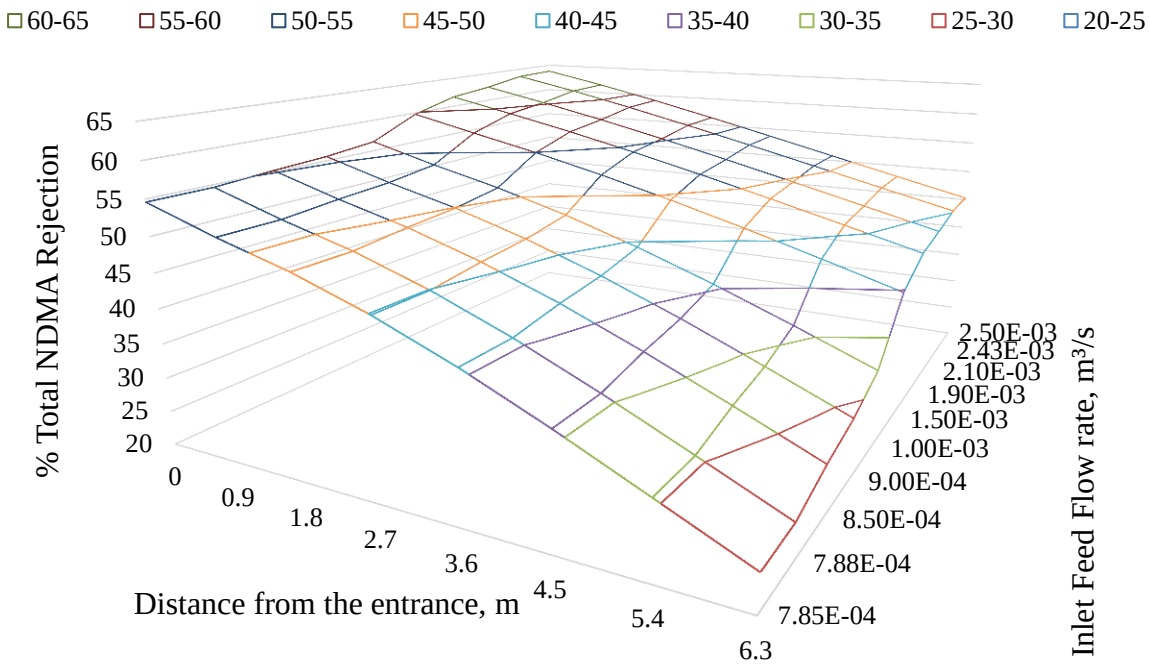

Fig. 12. The progress of NDMA rejection along a series of seven RO elements (inlet feed conditions: 10 atm, 250E-6 ppm and 20 ºC)

From the above analysis, it appears that the challenge of determining the best operating conditions that can guarantee the highest NDMA rejection of the selected configuration remains. This will require a careful and thorough investigation accounting for the conflicting impacts of the operating conditions. It is hoped that this study has paved the way for enhancing the understanding of how to select the optimum conditions in order to secure the optimum NDMA rejection for the selected RO layout.

7. Conclusions

This paper has analysed the feasibility of a full-scale spiral wound reverse osmosis consisting of seven series modules to remove NDMA from wastewater. A detailed simulation study has been used to investigate process performance under a wide range of operating parameters of feed pressure, flow rate, and concentration. This research yields the following key findings:

1. The maximum total NDMA rejection is always achieved at the highest feed flow rate tested regardless of the operating pressure.

2. The underlying layout can perform a maximum of 55.1% NDMA rejection at the tested operating conditions of 18 atm and 370E-6 ppm of feed pressure and concentration respectively.
3. The total NDMA rejection increases as a result of an increase in the inlet feed pressure especially at low feed flow rates conditions compared to a small reduction at high feed flow rates.
4. The total NDMA rejection is closely linked to:
    a) the feed flow rate with a small negative impact of feed concentration when the process is operating at low feed pressures, where the maximum rejection occurs at low feed concentrations.
    b) the feed flow rate with an insignificant negative impact of feed concentration when the process is operating at medium feed pressure, where the maximum rejection occurs at specific feed concentration.
    c) the feed concentration with a little positive impact of feed flow rate when the process is operating at high feed pressure, where the maximum rejection occurs at the highest feed concentration and flow rate.

The remaining issue of lower NDMA rejection requires further work to investigate the best RO network design and operating conditions in order to achieve the most feasible NDMA rejection, one that higher than the one achieved by a series configuration of seven elements.

Nomenclature

A_w : Solvent transport coefficient (m/atm s)

b : Feed and permeate channels friction parameter (atm s/m^4)

B_s : Solute transport coefficient (m/sec)

$C_{s(x)}$: Solute concentration in any point along the x-axis of the feed channel (kmol/m^3)

$C_{s(0)}$: Inlet solute concentration of the feed channel (kmol/m^3)

$C_{s(L)}$: Outlet solute concentration of the feed channel (kmol/m^3)

$C_{p(av)}$: Average permeate solute concentration in the permeate channel (kmol/m^3)

$C_{p(0)}$: Inlet permeate solute concentration of the permeate channel (kmol/m³)

$C_{p(L)}$: Outlet permeate solute concentration of the permeate channel (kmol/m³)

$C_{w(x)}$: Solute concentration at the membrane wall in any point along the x-axis of the feed channel (kmol/m³)

D_b : Diffusivity coefficient of solute (m²/s)

$F_{b(x)}$: Feed flow rate in any point along the x-axis of the feed channel (m³/s)

$F_{b(0)}$: Inlet feed flow rate of the feed channel (m³/s)

$F_{b(L)}$: Outlet feed flow rate of the feed channel (m³/s)

$F_{p(L)}$: Total Permeated flow rate (m³/s)

$F_{p(x)}$: Permeate flow rate in any point along the x-axis of the permeate channel (m³/s)

$J_{s(x)}$: Solute molar flux in any point along the x-axis of the feed channel (kmol/m² s)

$J_{w(x)}$: Water flux in any point along the x-axis of the feed channel (m/s)

$k_{(x)}$: Mass transfer coefficient in any point along the x-axis of the feed channel (m/s)

K : The efficiency of mixing net (i.e. spacer), (K = 0.5)

L : Length of the membrane (m)

$m_{f(x)}$: Parameter defined in Eq. (12)

$P_{b(x)}$: Feed pressure in any point along the x-axis of the feed channel (atm)

$P_{b(0)}$: Inlet feed pressure of the feed channel (atm)

$P_{b(L)}$: Outlet feed pressure of the feed channel (atm)

P_p : Permeate pressure at the permeate channel (atm)

R : Gas low constant $\left(\mathrm{R} = 0.082 \frac{\mathrm{atm\ m^3}}{\mathrm{K\ kmol}}\right)$

$Rec_{(Total)}$: Total water recovery coefficient (dimensionless)

Rej : Solute rejection coefficient (dimensionless)

$Re_{(av)}$: Average Reynolds number along the membrane length (dimensionless)

$Re_{(x)}$: Reynolds number in any point along the x-axis of the feed channel (dimensionless)

T_b : Feed temperature (°C)

t_f : Feed spacer thickness (m)

t_p : Permeate spacer thickness (m)

$U_{b(x)}$: Feed velocity in any point along the x-axis of the feed channel (m/s)

x : Point of length at x-axis of the membrane under consideration (m)

W : Width of the membrane (m)

θ : Parameter defined in Eq. (2)

$\mu_{b(x)}$: Dynamic viscosity parameter in any point along the x-axis of the feed channel (kg/m s)

$\rho_{b(x)}$: Feed density parameter in any point along the x-axis of the feed channel (kg/m³)

ΔL : Characteristic length of mixing net (m)

$\Delta P_{b(0)}$: Pressure difference at inlet edge of membrane (atm)

$\Delta P_{b(x)}$: Pressure difference in any point along the x-axis (atm)

Δx : Length of sub-section (m)

References

[1] Drioli E, Fontananova E. Membrane technology and sustainable growth. *Chem Eng Res Des*, 2004; 82(12): 1557-1562.

[2] Fritzmann C, Löwenberg J, Wintgens T, Melin T. State-of-the-art of reverse osmosis desalination. *Desalination*, 2007; 216: 1-76.

[3] Song L, Hong S, Hu J, Ong S, Ng W. Simulations of Full-Scale Reverse Osmosis Membrane Process. *J Environ Eng*, 2002; 128(10): 960.

[4] Du Y, Xie L, Wang Y, Xu Y, Wang S. Optimization of reverse osmosis networks with spiral-wound modules. *Ind. Eng. Chem. Res.* 2012; 51: 11764-11777.

[5] Selbes M, Glenn M, Karanfil T. The Role of Pre-Oxidation in Controlling NDMA Formation: A Review. *Recent Advances in Disinfection By-Products*. American Chemical Society; January 1, 2015, 151-172, Chapter DOI:10.1021/bk-2015-1190.ch009

[6] Krauss M, Longrée P, Van Houtte E, Cauwenberghs J, Hollender J. Assessing the fate of nitrosamine precursors in wastewater treatment by physicochemical fractionation. *Environ. Sci. Technol*. 2010; 44: 7871-7877.

[7] Fujioka T, Khan SJ, Mcdonald JA, Roux A, Poussade Y, Drewes JE, Nghiem LD. Modelling the rejection of N-nitrosamines by a spiral-wound reverse osmosis system: Mathematical model development and validation. *J Membr Sci*, 2014; 454**:** 212-219.

[8] Al-Obaidi M, Mujtaba IM. Development and validation of N-nitrosamine rejection mathematical model using a spiral wound reverse osmosis process. *Chem. Eng. Trans.* 2016; 52: 1129-1134.

[9] Kostoglou M, Karabelas AJ. Mathematical Analysis of the Meso-Scale Flow Field in Spiral-Wound Membrane Modules. *Ind. Eng. Chem. Res.* 2011; 50: 4653-4666.

[10] Al-Obaidi MA, Li J- P, Kara-Zaïtri C, Mujtaba IM. Optimisation of reverse osmosis based wastewater treatment system for the removal of chlorophenol using genetic algorithms. *Chem Eng J,* 2017; 316: 91-100.

[11] Mane PP, Park P-K, Hyung H, Brown JC Kim J-H. Modelling boron rejection in pilot- and full-scale reverse osmosis desalination processes. *J Membr Sci*, 2009; 338**:** 119-127.

[12] Koroneos C, Dompros A, Roumbas G,. Renewable energy driven desalination systems modelling. *J. Cleaner Prod.* 2007; 15: 449-464.

[13] Lee C, Chen Y, Wang G. A dynamic simulation model of reverse osmosis desalination systems. The 5th International Symposium on Design, Operation and Control of Chemical Processes, PSE ASIA, Singapore, 2010.

[14] Process System Enterprise Ltd., 2001. gPROMS Introductory User Guide. London: Process System Enterprise Ltd.

[15] Sutzkover I, Hasson D, Semiat R. Simple technique for measuring the concentration polarization level in a reverse osmosis system. *Desalination*, 2000; 131: 117-127.

[16] Steinle-Darling E, Zedda M, Plumlee MH, Ridgway HF, Reinhard M. Evaluating the impacts of membrane type, coating, fouling, chemical properties and water chemistry on reverse osmosis rejection of seven nitrosoalklyamines, including NDMA. *Water Res*, 2007; 41: 3959-3967.

[17] Plumlee MH, Lo´pez-Mesas M, Heidlberger A, Ishida KP, Reinhard M. N-nitrosodimethylamine (NDMA) removal by reverse osmosis and UV treatment and analysis via LC–MS/MS. *Water Res*, 2008; 42: 347-355.

[18] Haluch V, Zanoelo EF, Hermes CJL. Experimental evaluation and semi-empirical modeling of a small-capacity reverse osmosis desalination unit. *Chem Eng Res Des*, 2017: 122; 243-253.

[19] Al-Obaidi M, Mujtaba IM. Steady state and dynamic modeling of spiral wound wastewater reverse osmosis process. *Comput Chem Eng*, 2016; 90: 278-299.

[20] Gómez J, León G, Hidalgo A, Gómez M, Murcia M, Griñán G. Application of reverse osmosis to remove aniline from wastewater. *Desalination*, 2009; 245: 687-693.